Authors' accepted manuscript.
Article published in *Metallurgical and Materials Transactions A* vol. 51, pages 5617–5622 (2020)
The final published version is available at https://doi.org/10.1007/s11661-020-05975-y

The Effect of Retained Work Hardening on the Driving Force for Dynamic Transformation

- K. Chadha,
- C. Aranas Jr.,
- D. Shahriari,
- M. Jahazi &
- J. G. Spray

Metallurgical and Materials Transactions A **volume 51**, pages5617–5622 (2020)

- DOI https://doi.org/10.1007/s11661-020-05975-y

Authors' accepted manuscript.
Article published in *Metallurgical and Materials Transactions A* vol. 51, pages 5617–5622 (2020)
The final published version is available at https://doi.org/10.1007/s11661-020-05975-y

The Effect of Retained Work Hardening on the Driving Force for Dynamic Transformation

K. Chadha[1*], C. Jr. Aranas[2], D. Shahriari[3], M. Jahazi[3], J.G. Spray[1]

[1]Planetary and Space Science Centre, University of New Brunswick
Fredericton, New Brunswick E3B 5A3, Canada
[2]Department of Mechanical Engineering, University of New Brunswick
Fredericton, New Brunswick E3B 5A3, Canada
[3]Department of Mechanical Engineering, École de technologie supérieure (ÉTS),
1100 Notre Dame Street West, Montréal, Québec H3C 1K3, Canada

*Corresponding Author: kchadha@unb.ca

The driving force for dynamic transformation during double-hit hot compression of an as-cast medium-carbon low-alloy steel was done at 1473 K at strain rates of 0.25 s^{-1} and 0.50 s^{-1}. Dynamically transformed ferrite was detected using the Kernel Average Misorientation (KAM) technique. The time interval between deformations affects the retained driving force, which decreases at a rate of 65-75 J/mol per second. This rate decreases with decreasing temperature due to a lower rate of recovery.

Keywords: Dynamic Transformation; Thermomechanical Processing; Double-hit Hot Compression

The high-temperature deformation of steels is known to induce the austenite to ferrite phase transformation at temperatures above the Ae_3 [1,2]. This transformation may affect the mechanical properties of the final product following hot deformation and any subsequent processing. For example, this mechanism contributes to the production of high-strength steels with fine-grain microstructure, as shown in Ref. [3] and [4]. However, despite the benefits of dynamic transformation

(DT), consideration of this phenomenon is often neglected in the thermomechanical modeling of hot forming processes such as rolling or forging [5,6]. This is because of the complex nature of DT, and/or the limited understanding of the exact effects of multi-pass deformation on its occurrence.

To date, several papers have provided in-situ evidence of dynamic transformation (DT) employing neutron diffraction and synchrotron techniques [7,8]. There are also thermodynamic models to support the occurrence of this type of phase transformation [9-11]. These models show that either (1) the stored energy of dislocations or (2) transformation softening act as driving forces to induce the phase transformation. The former cannot explain the dynamic phase transformation that takes place well above the Ae_3 temperature (100 °C or more above the Ae_3 [1,2,12], while the latter does support the transformation. Although there are numerous experimental and theoretical studies on DT, the effect of *multi-pass* deformation on the driving force to initiate DT has not been explored despite the fact that most of the industrial hot deformation operations are multi-pass by nature. The retained stress after each pass affects the driving force, and therefore needs to be taken into consideration. The present work provides a method to incorporate the retained stress in the calculation of driving force during multi-pass deformation. An as-cast medium-carbon low-alloy steel was employed for this purpose.

The composition of the steel used for the experiments is shown in **Table 1,** along with its para-equilibrium temperature. These values were calculated using the FactSage thermodynamic software [13]. Materials were provided by Finkl Steel-Sorel. Cylindrical specimens were machined from the central region of the as-cast ingot with diameters and heights of 10 mm and 15 mm, respectively. Hot compression tests were performed using a Gleeble 3800® thermomechanical simulator following the procedures described in ASTM E209. The schematic diagram for double-hit compression tests is shown in **Fig. 1**. One temperature (1473 K/1200 °C), two strain rates (0.25 s^{-1} and 0.5 s^{-1}), and one interpass time (5 s) were employed in the experiments.

Table 1. Composition of as-cast medium-carbon low-alloy steel.

C	Mn	Si	Mo	Cr	Other	$Ae_{3(p)}$
0.35	0.84	0.41	0.44	1.90	Microalloying	759°C

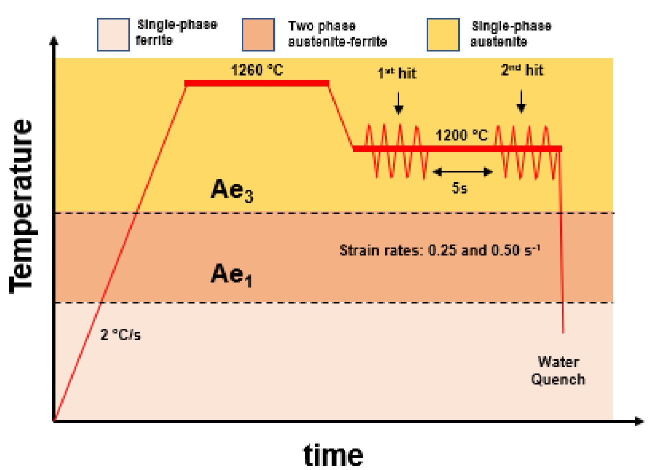

Figure 1. Schematic diagram of thermomechanical schedule for hot compression tests of as-cast medium-carbon low-alloy steel.

The thermomechanical procedure consisted of heating the sample to 1533 K (1260 °C) at a heating rate of 2 °C/s and soaking for 5 minutes (300 s) to homogenize the temperature and the microstructure. The samples were then cooled to the deformation temperature at a rate of 1 °C/s before being compressed to a total true strain of 0.8. The first deformation was applied at a true strain of 0.5 followed by 5 s interpass time. The second pass was then applied at a true strain of 0.3 followed by water quenching. All tests were conducted at least 3 times in order to evaluate the variations, which were found to be less than 5%. The samples were mechanically polished using conventional metallographic preparation techniques and final polished using a Vibromet® polisher. The EBSD analysis was performed using a Hitachi SU-70 field emission gun scanning electron microscope equipped with Schottky emitter. Post-processing was done using the TSL-OIM™ software.

The flow curves obtained from the double-hit deformation at 1473 K (1200 °C) and strain rates of 0.25 s^{-1} and 0.5 s^{-1} and the interpass time of 5s are displayed in **Fig. 2 a**. Note that this temperature is approximately 723 K (450 °C) above the para-equilibrium Ae_3 temperature of the investigated alloy. As expected, the results show that the stress levels increase with an increase in strain rate. After the first deformation, both flow curves show a steady increase in stress and then gradually decrease after a peak stress of 58 MPa and 63 MPa for strain rates of 0.25 s^{-1} and 0.5 s^{-1}, respectively. During the second deformation, a peak stress drop of approximately 15% (compared to the first deformation) can be observed for both testing conditions, i.e., peak stresses of 50 MPa and 54 MPa were recorded for strain rates of 0.25 s^{-1} and 0.5 s^{-1}, respectively. These results indicate that softening mechanisms such as metadynamic recrystallization or static recrystallization [14,15] have taken place in the 5 s time interval. The double differentiation calculations were carried out using a MATLAB® script to assess the occurrence of dynamic recrystallization (DRX) and DT. The MATLAB® was developed using Levenberg-Marquardt algorithm and considering the degree of polynomial 'n' higher than 8th order. The details of the analysis technique could be found in the following references [1,16-21].

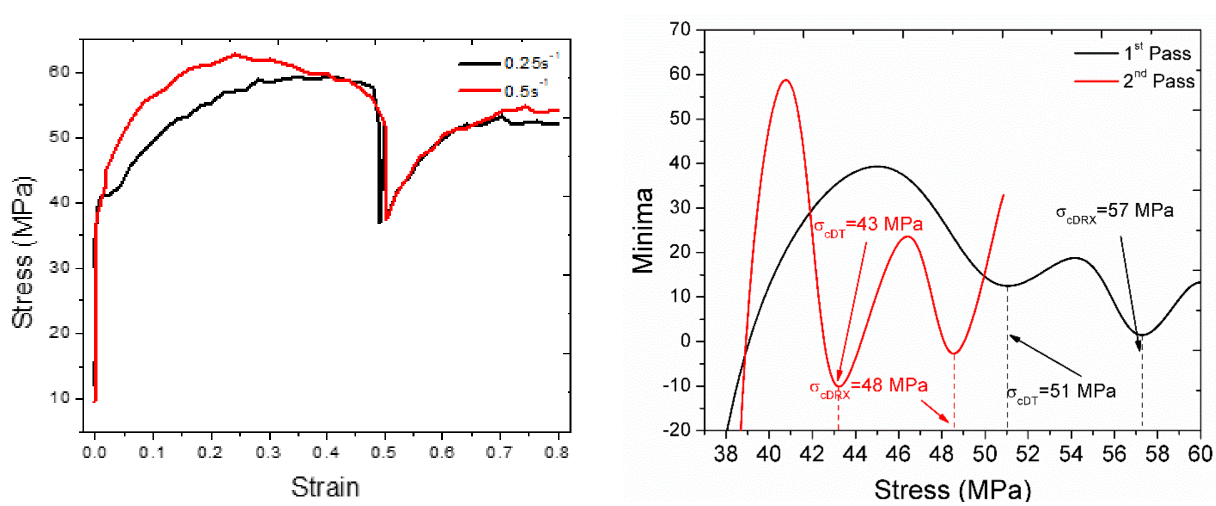

(a) (b)

Figure 2. (a) Stress Strain curve of as-cast medium-carbon low-alloy steel deformed at 1473 K (1200 °C) and strain rates of 0.25 s^{-1} and 0.5 s^{-1} with an interpass time of 5s. (b) Double Differential minima curves at deformation temperature of 1473 K (1200 °C) and strain rate of 0.25 s^{-1}

The first and second minima in each curve of **Fig. 2 b** represent the critical stresses at which DT and DRX were initiated during deformation, respectively [22-24]. From the figure, we can observe that the critical stresses during second deformation are lower than the first deformation (see **Table 2**). This can be due to the retained stress after the first pass, which provides part of the driving force needed to re-initiate DT. Since double differentiation technique involves purely mathematical findings, microstructural analysis is needed to validate the presence of dynamically transformed ferrite, as presented below.

Fig. 3 shows the grain boundary map of the specimen after double hit deformation at 1473 K (1200 °C) and strain rates of 0.25 s^{-1} (**Fig. 3 a**) and 0.5 s^{-1} (**Fig. 3 b**). The microstructure shows prior austenite grain boundaries, confirming its large grain size. A close observation of the microstructures reveals a morphology composed of laths and few quasi-polygonal grains (shown with red and yellow arrows). The plates observed in the microstructure appear to have Widmanstaetten type morphology in the plane containing the compression direction, which originates from the interior of the grains. This observation is consistent with the results of numerous researchers [1,12,25] who related their formation to the applied stress, which induces the displacive transformation of austenite to Widmanstaetten ferrite. More specifically, Ghosh et al. [26] performed an atom probe tomography studies to confirm such morphology. This morphology might be different from the plane normal to the compression direction, which is probably due to variant selection in the texture as a consequence of applied stress [27]. A comparative observation of the features of the microstructure at the two applied strain rates, **Fig. 3 a** and **Fig. 3 b**, revealed that the Widmanstaetten ferrite plates and quasi-polygonal plates were finer at 0.5 s^{-1} strain rate. There is also significant number of low-angle grain boundaries present in both microstructures which indicates that the microstructure is not fully recovered after the second hit. However, no indication of LAGBS was found in the laths and plates, which suggests that these grains underwent recrystallization (due to bulging as shown with black arrows) and phase transformation. The fraction of LAGBS in 0.5 s^{-1} (62%) was higher than that of 0.25 s^{-1} (34%) by approximately 50%. This observation may be due to the higher recovery time for the lower strain rates.

Table 2. Critical Stresses for DT and DRX for deformation temperature of 1473 K (1200 °C) and strain rate of 0.25 s^{-1} and 0.5 s^{-1} with interpass time of 5s.

Strain Rate	First hit		Second Hit	
	DT	DRX	DT	DRX
0.25s^{-1}	51	57	43	48
0.5s^{-1}	48	55	43	48

Since it is difficult to differentiate martensite and DT ferrite using XRD, optical microscopy, or secondary electron imaging, the present study employed the Kernal Average Misorientation (KAM) method [17]. In this approach, internal misorientation between grains is used to distinguish the martensite (body-centered tetragonal) from the ferrite (body-centered cubic) by means of EBSD images. Up to the third nearest neighbor was considered for calculating KAM values, and a threshold angle of 5° was employed. It is known that ferrite has a higher stacking fault energy (SFE) than austenite [28], which would make dynamic recovery easier when it is further deformed to a higher strain (ε=0.8). On the other hand, martensite laths (from untransformed austenite), which are formed due to shape deformation (displacive transformation), generate a higher amount of LAGBs, resulting in higher misorientations within the laths. Therefore, the area fractions with less than 2° misorientation (i.e., KAM ≤ 2°; green and blue regions) were considered as ferrite and more than 2° misorientation as martensite (yellow and red regions). Using the above criteria, the dynamic recovery process of the two phases was studied, and differentiation was successfully made between ferrite and martensite.

Fig. 3 c shows the KAM map for the specimen deformed at 1473 K (1200 °C) and at a strain rate of 0.25 s^{-1}. Widmanstaetten ferrite plates (marked as WF) , as observed on the Grain Boundary map of **Figs. (3 a & b)**, have <2° misorientation, thus confirming that they are recovered ferrite grains. On the other hand, grains with KAM values between 3°-5° indicate the presence of martensite. The volume fractions of ferrite (i.e. grains with <2° misorientation) are 62% and 40% for 0.25 s^{-1} and 0.5 s^{-1}, respectively. As expected, the amount of ferrite increases as the strain rate decreases due to larger diffusion distances of the alloying elements [18].

The presence of ferrite after double-hit deformation can be attributed to the increase in the free energy of austenite during straining, which leads to the higher thermodynamic stability of ferrite [11]. As shown in Ref. [29], the driving force for dynamic transformation is obtained by taking the difference between the DT critical stress and the yield stress of the fresh ferrite that takes place as described by equation 1 below:

$$E_{DF} = \sigma_c - \sigma_{\alpha\text{-}YS} \qquad (1)$$

where E_{DF} is the driving force, σ_c is the DT critical stress, and $\sigma_{\alpha\text{-}YS}$ is the yield stress for ferrite. Note that the stress values can be converted into stored energy, as shown in in the literature[2]. All the measured stresses in the first pass came from fully austenitic phase; thus, the stress values are associated with austenite. For the second pass, due to difficulty in separating the individual stresses of ferrite and austenite in the present work, it is assumed that most of the ferrite formed in the first pass either retransformed back into austenite or negligible enough to significantly affect the stress levels.

Since the yield stress of fresh ferrite at 1473 K (1200 °C) cannot be measured experimentally, this was estimated using JMatPro materials property simulation software (version 11) employing the general steel module. The yield stress employed in this work is 11.5 MPa. It is well known that if the driving force is greater than the total obstacle energy, then a dynamic phase transformation can take place. The total energy barrier can be calculated using the equation below:

$$E_B = \Delta G_{\gamma\text{-}\alpha} + W_D + W_{SA} \qquad (2)$$

where E_B is the total energy barrier, $\Delta G_{\gamma\text{-}\alpha}$ is the Gibbs energy difference between austenite and ferrite (219 J/mol), W_D is the required work of dilatation to transform austenite into ferrite, and W_{SA} is the required shear accommodation work during the phase transformation. The values of W_D and W_{SA} are dependent on the critical stresses, which can be calculated using the following equations:

$$W_D = \sigma_c \times m \times 0.03 \times 7.2 \text{ (J/mol)} \quad (3)$$

$$W_{SA} = \sigma_c \times \sqrt{m} \times 0.22 \times 7.2 \text{ (J/mol)} \quad (4)$$

where m is the Schmid factor, 0.03 and 0.22 are the required lattice and shear accommodation strains to displacively transform austenite into ferrite, and 7.2 is a conversion factor[29]. Note that equations 2, 3 and 4 assumes that the austenite grains with the highest Schmid factor (i.e., the orientation of the transformation habit plane and shear direction with respect to the loading direction), wherein m = 0.5, will initially transform. The transformation of most oriented grains is directly associated with the DT critical stresses as reported in the literature [7]. In this work, the total obstacle energy is based on the average critical stress of both strain rates during the first pass (49 MPa), where a single austenite phase is expected. The values of W_D and W_{SA} are 7.6 and 39.2 J/mol, respectively.

Using the data from Table 2 and the free energy difference between austenite and ferrite, and the estimated yield stress of ferrite at 1473 K (1200 °C), the driving forces and total energy barrier during double-hit deformation are obtained (**Fig. 4 a)**. The total obstacle energy to transform the austenite grains into ferrite at 1473 K (1200 °C) is estimated at 265 J/mol. For the experiment with the strain rate of 0.25 s^{-1}, the driving force for DT after the first deformation is about 275 J/mol, a value slightly higher than the total obstacle energy. Similarly, for the experiment with the strain rate of 0.5 s^{-1}, the calculated driving force is also higher than the total obstacle energy, which is 268 J/mol. These observations show that the calculated first deformation critical stresses using the double differentiation method seem to reflect the exact moment of transformation from austenite to ferrite.

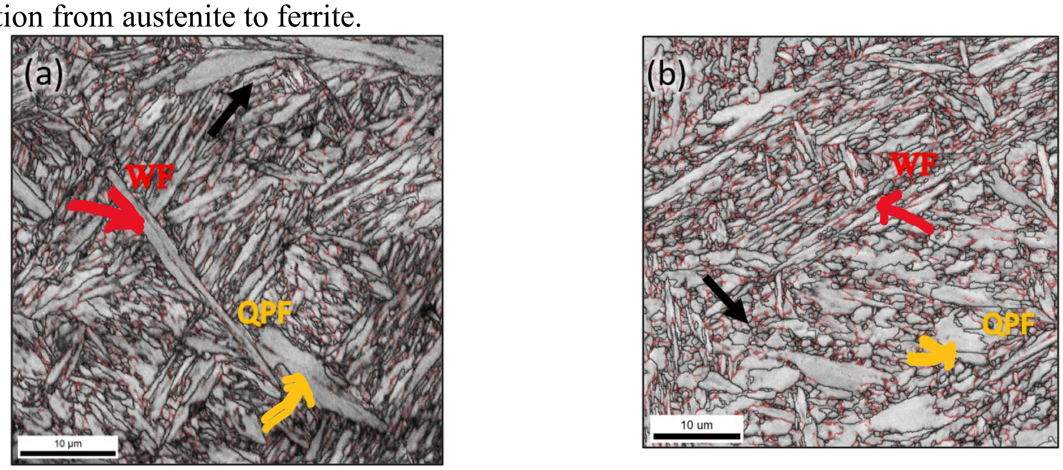

(a) (b)

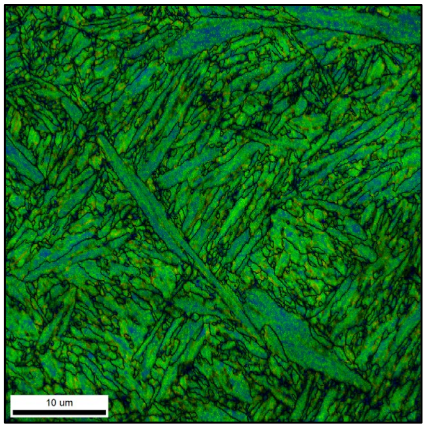

(c)

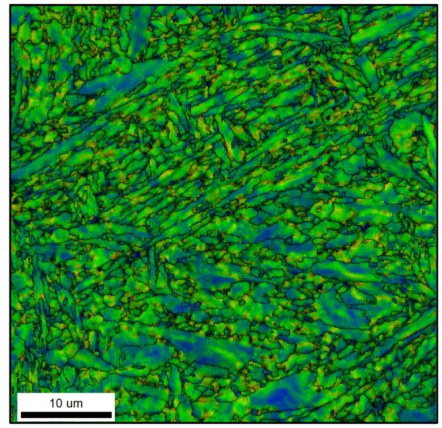

(d)

Figure 3. EBSD grain boundary map of as-cast medium-carbon low-alloy steel deformed at deformation temperature of 1473 K (1200 °C) and strain rate of (a) 0.25 s^{-1}, (b) 0.5 s^{-1} . The black encircled region shows the disintegration of the Widmanstaetten plate at high strain rate. EBSD Kernal Average Map (KAM) of as-cast medium-carbon low-alloy steel deformed at deformation temperature of 1473 K (1200 °C) at strain rate of (c) 0.25 s^{-1}, (d) 0.5 s^{-1}. Low-angle grain boundaries (LAGB's, θ >2°) are marked red, while high-angle grain boundaries (HAGB's, θ > 15°) are labeled black.

Although the first deformation driving force values perfectly align with the observations in the literature [16], the calculated driving forces in the second deformation employing strain rates of 0.25 s^{-1} and 0.50 s^{-1} were significantly lower than the total energy barrier (224 J/mol and 229 J/mol, respectively). Note that DT has been previously shown to take place every pass during rolling, and the interpass time affects the volume fraction of DT ferrite [18]; thus, in the present work, it seems that the retained work hardening in between deformation plays a significant role in supplying a retained driving force to re-initiate DT in the second deformation. More specifically, the experiments with strain rates of 0.25 s^{-1} and 0.5 s^{-1} require additional driving forces of at least 41 J/mol and 36 J/mol, respectively, to initiate dynamic phase transformation, as displayed in **Fig. 4 a**.

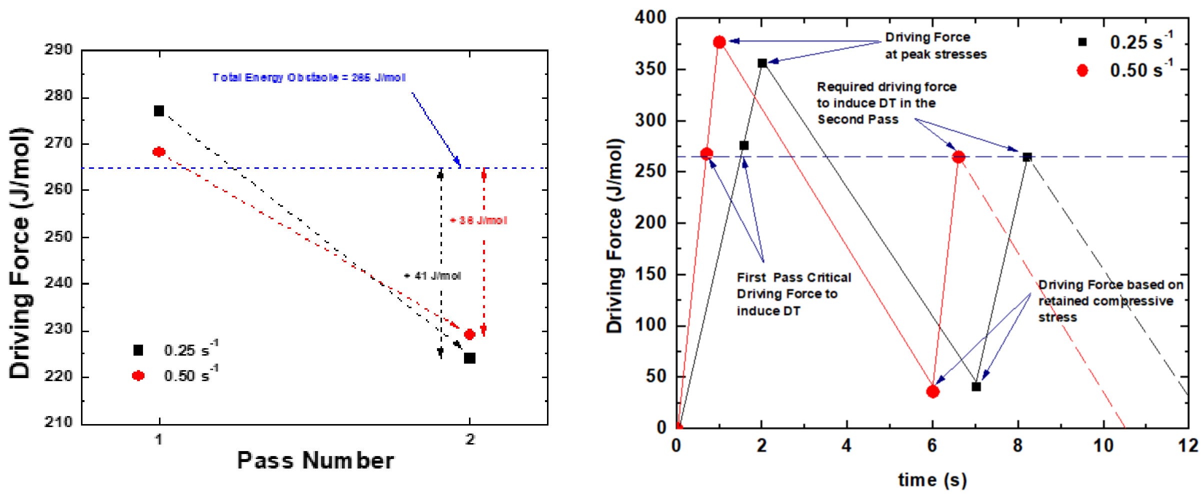

(a) (b)

Figure 4. (a) Driving force and Total Energy Barrier during deformation at 1473 K (1200 °C) and strain rates of 0.25 s^{-1} and 0.5 s^{-1} with an interpass time of 5s. (b) Dependence of the driving force on the progression of deformation at 1473 K (1200 °C) and strain rates of 0.25 s^{-1} and 0.5 s^{-1} with an interpass time of 5s.

The dependence of the driving force on the progression of double-hit experiments was tracked and plotted (**Fig. 4 b)**. To better understand the time scale in this figure, note that the time it takes to complete the first deformation for strain rate of 0.25 s^{-1} is only 2 s (see the black lines). Since the interpass time is 5 s, the 2nd deformation starts after 7 s, which takes about 1.2 s to complete. The whole process of 0.25 s^{-1} test ends after 8.2 s. The square markers denotes the time where the critical, peak and retained compressive stresses are achieved. Similarly, for strain rate of 0.50 s^{-1} (see red line), the first deformation is completed within 1 s, followed by interpass time of 5 s. The second deformation starts after 6 s, which will only last for 0.6 second. The duration of the 0.50 s^{-1} test is 6.6 seconds. The red circle markers provide important stress values associated with DT, which are explained below.

During the first deformation, the critical driving forces were detected after 0.7s (268 J/mol) and 1.6s (275 J/mol) for experiments employing strain rates of 0.25 s^{-1} and 0.5 s^{-1}, respectively. At the peak stress, where the driving force is at its maximum, the driving forces in the material are 375 J/mol (at 1s) and 356 J/mol (at 2s) for strain rates of 0.25 s^{-1} and 0.5 s^{-1}, respectively. There is a retained stored energy (from compressive stress) in the material before the second deformation (during the interpass time), followed by static recovery. This retained stress was tracked by not retracting the compression anvils after deformation to measure the amount of recovery in the material during interpass interval. In this experiment, the retained compressive stresses (which can be converted into a stored energy) after 5 s of holding are readily seen in the flow curves of **Fig. 2,** 37 MPa and 37 MPa for strain rates of 0.25 s^{-1} and 0.5 s^{-1}, respectively (see the initial values of the second deformation). These stresses were directly measured from the stress-strain curves. Based on this data, it appears that the retained compressive stress, which can be compared to the retained work hardening during the pass interval in hot rolling and forging processes, were able to provide the missing additional driving force specified above, which are 41 J/mol and 36 J/mol for strain rates of 0.25 s^{-1} and 0.5 s^{-1}, respectively. Thus, for the strain rate of 0.25 s^{-1}, the driving force after 6 s is estimated at 36 J/mol (immediately before the second deformation), while for the strain rate of 0.5 s^{-1}, the driving force after 7s is about 41 J/mol (also immediately before the second deformation). In this work, the estimated decrease in driving force at 1473 K (1200 °C) between deformations is 65-75 J/mol per second. It is expected that this rate decreases with decreasing temperature due to lower recovery rates at lower temperatures. Then, during the second deformation, the material acquired a driving force equal to that of the total obstacle energy (265 J/mol) after 6.6 s and 8.2 s for strain rates of 0.25 s^{-1} and 0.5 s^{-1}, respectively, to induce phase the transformation. These points are associated with the critical stresses observed during the second deformation.

In the present work a method was introduced to analyze the occurrence of DT and to track the amount of driving force during multi-pass high temperature deformation. The DT ferrite and martensite (prior austenite) were successfully distinguished using EBSD imagery employing the KAM method. For the first time, the DT driving force was determined and the conditions for the occurrence of DT during multi-deformation processing were quantitatively predicted.

The authors acknowledge with gratitude funding received from the Natural Sciences and Engineering Research Council of Canada (NSERC), New Brunswick Innovation Foundation (NBIF), Canada Foundation for Innovation (CFI) and Harrison McCain Foundation.

References

[1] C. Ghosh, C. Aranas Jr and J.J. Jonas: *Prog. Mater. Sci., 2016, vol.* 82, pp. 151-233.
[2] H. Yada, T. Matsumura, and T. Senuma: *THERMEC 88, Int. Conf. Physical Metallurgy of Thermomechanical Processing of Steels and Other Metals,* 1988, pp. 200–207.
[3] L. Zhao, N. Park, Y. Tian, A. Shibata and N. Tsuji: *Sci. Rep., vol.* 6, pp. 39127.
[4] B. Eghbali: *Mater. Sci. Eng. A, 2010, vol.* 527, pp. 3407-3410.
[5] C. Facusseh, A. Salinas, A. Flores and G. Altamirano: *Metals, 2019, vol.* 9, pp. 1289.
[6] X. Wang, K. Chandrashekhara, S.N. Lekakh, D.C. Van Aken and R.J. O'Malley: *Steel Res. Int., 2019, vol.* 90, pp. 1700565.
[7] C. Aranas Jr, S. Rodrigues, F. Siciliano and J. Jonas: *Scr. Mater., 2020, vol.* 177, pp. 86-90.
[8] A. Shibata, Y. Takeda, N. Park, L. Zhao, S. Harjo, T. Kawasaki, W. Gong and N. Tsuji: *Scr. Mater., 2019, vol.* 165, pp. 44-49.
[9] C. Ghosh, V.V. Basabe, J.J. Jonas, Y.-M. Kim, I.-H. Jung and S. Yue: *Acta Mater.,* 2013, vol. 61, pp. 2348-2362.
[10] J.J. Jonas and C. Ghosh: *Acta Mater, 2013, vol.* 61, pp. 6125-6131.
[11] C. Aranas Jr and J.J. Jonas: *Acta Mater., 2015, vol* 82, pp. 1-10.
[12] R. Grewal, C. Aranas Jr, K. Chadha, D. Shahriari, M. Jahazi and J.J. Jonas: *Acta Mater, 2016, vol.* 109, pp. 23-31.
[13] C. Bale, E. Bélisle, P. Chartrand, S. Decterov, G. Eriksson, K. Hack, I.-H. Jung, Y.-B. Kang, J. Melançon and A. Pelton: *Calphad*, 2009, vol. 33, pp. 295-311.
[14] K. Chadha, D. Shahriari and M. Jahazi: *MATEC Web Conf.*, 2016, vol. 80, pp. 06004.
[15] S.-H. Cho, K.-B. Kang and J.J. Jonas: *ISIJ Int., 2001,* vol. 41, pp. 63-69.
[16] C. Aranas Jr, T. Nguyen-Minh, R. Grewal and J.J. Jonas: *ISIJ Int., 2015, vol.* 55, pp. 300-307.
[17] K. Chadha, Z. Ahmed, C. Aranas Jr, D. Shahriari and M. Jahazi: *Materialia*, 2018, vol. 1, pp. 155-167.

[18] K. Chadha, D. Shahriari, C.J. Aranas, L.-P. Lapierre-Boire and M. Jahazi: *Met. Mater. Int.,* 2019, vol. 25, pp. 559-569.
[19] E.I. Poliak and J.J. Jonas: *ISIJ Int.,* 2003, vol. 43, pp. 692-700.
[20] E. Poliak and J. Jonas: *Acta Mater.,* 1996, vol. 44, pp. 127-136.
[21] J.J. Jonas, C. Ghosh, X. Quelennec and V.V. Basabe: *ISIJ Int.,* 2013, vol. 53, pp. 145-151.
[22] C. Ghosh, V.V. Basabe and J.J. Jonas: *Steel Res. Int.,* 2013, vol. 84, pp. 490-494.
[23] X. Sun, H. Luo, H. Dong, Q. Liu and Y. Weng: *ISIJ Int.,* 2008, vol. 48, pp. 994-1000.
[24] J.-K. Choi, D.-H. Seo, J.-S. Lee, K.-K. Um and W.-Y. Choo: *ISIJ Int.,* 2003, vol. 43, pp. 746-754.
[25] N. Park, A. Shibata, D. Terada and N. Tsuji: *Acta Mater.,* 2013, vol. 61, pp. 163-173.
[26] C. Ghosh, V.V. Basabe, J.J. Jonas, S. Yue and X.Y. Xiong: *ISIJ Int,* 2013, vol. 53, pp. 900-908.
[27] J.J. Jonas, Y. He and G. Langelaan: *Acta Mater.* 2014, vol. 72, pp. 13-21.
[28] W. Reick, M. Pohl and A.F. Padilha: *ISIJ Int., 1998,* vol. 38, pp. 567-571.
[29] C. Aranas Jr, S. Rodrigues, A. Fall, M. Jahazi and J.J. Jonas: *Metals,* 2018, vol. 8, pp. 360.